



**EUROfusion**

WPMAG-CPR(17) 17835

R Bonifetto et al.

# **Thermal-hydraulic test of the ENEA TF conductor sample for the EU DEMO fusion reactor**

Preprint of Paper to be submitted for publication in Proceeding of  
13th European Conference on Applied Superconductivity



This work has been carried out within the framework of the EUROfusion Consortium and has received funding from the Euratom research and training programme 2014-2018 under grant agreement No 633053. The views and opinions expressed herein do not necessarily reflect those of the European Commission.

This document is intended for publication in the open literature. It is made available on the clear understanding that it may not be further circulated and extracts or references may not be published prior to publication of the original when applicable, or without the consent of the Publications Officer, EUROfusion Programme Management Unit, Culham Science Centre, Abingdon, Oxon, OX14 3DB, UK or e-mail [Publications.Officer@euro-fusion.org](mailto:Publications.Officer@euro-fusion.org)

Enquiries about Copyright and reproduction should be addressed to the Publications Officer, EUROfusion Programme Management Unit, Culham Science Centre, Abingdon, Oxon, OX14 3DB, UK or e-mail [Publications.Officer@euro-fusion.org](mailto:Publications.Officer@euro-fusion.org)

The contents of this preprint and all other EUROfusion Preprints, Reports and Conference Papers are available to view online free at <http://www.euro-fusionscipub.org>. This site has full search facilities and e-mail alert options. In the JET specific papers the diagrams contained within the PDFs on this site are hyperlinked

# Thermal–hydraulic test and analysis of the ENEA TF conductor sample for the EU DEMO fusion reactor

R. Bonifetto, P. Bruzzone, V. Corato, L. Muzzi, *Senior Member, IEEE*, L. Savoldi, *Member, IEEE*, B. Stepanov, R. Zanino, *Senior Member, IEEE*, A. Zappatore

**Abstract**—The ENEA conductor for the EU DEMO Nb<sub>3</sub>Sn Toroidal Field (TF) magnets, cooled by supercritical He, features a rectangular cross section with two small pressure relief channels (“holes”), separated from the cable bundle by means of a flat spiral, twisted together with the last cabling stage. A well instrumented short sample of the ENEA TF conductor has been tested in SULTAN at SPC, Villigen (Switzerland) in 2016, aimed at its thermal-hydraulic characterization, and the test results are presented here. A correlation for the friction factor in the small holes is derived, best fitting the results of a set of computational- fluid dynamics (CFD) experiments. The new correlation (combined with existing correlations for the He friction factor in the bundle region) is shown to allow a proper reproduction of the measured hydraulic characteristic of the conductor. The heat slug propagation tests are used to calibrate the hole-to-bundle heat transfer coefficient in the 4C thermal-hydraulic code and to estimate the characteristic length for the homogenization of the He temperature on the conductor cross section, following a localized thermal perturbation.

**Index Terms**—CFD, CICC thermal-hydraulic characterization, DEMO, superconductor sample test.

## I. INTRODUCTION

THE superconducting (SC) magnet system of the EU DEMO fusion reactor is currently in the pre-conceptual design phase within the Magnets Work Package (WPMAG) [1], [2]. Three options have been considered up to now for the toroidal field coils, based on low-temperature SC cable-in-conduit conductor (CICC) cooled by supercritical He. In the ENEA option [3], two out of six cable petals of this CICC are obtained twisting the strands around a low-impedance spiral-walled channel (“hole”), see Fig. 1, similarly to what is proposed for some of the Korean DEMO conductors [4].

This work has been carried out within the framework of the EUROfusion Consortium and has received funding from the Euratom research and training programme 2014-2018 under grant agreement No 633053. The views and opinions expressed herein do not necessarily reflect those of the European Commission. (*Corresponding author: R. Bonifetto.*)

R. Bonifetto, L. Savoldi, R. Zanino, and A. Zappatore are with the NEMO Group, Dipartimento Energia, Politecnico di Torino, 10129 Torino, Italy (e-mail: roberto.bonifetto@polito.it, laura.savoldi@polito.it, roberto.zanino@polito.it, andrea.zappatore@polito.it).

P. Bruzzone and B. Stepanov are with SPC EPFL, Villigen 5232, Switzerland (e-mail: pierluigi.bruzzone@psi.ch, boris.stepanov@psi.ch).

V. Corato and L. Muzzi are with ENEA, 00044 Frascati, Italy and also with Italian Consortium for Applied Superconductivity (ICAS), 00044 Frascati, Italy (e-mail: valentina.corato@enea.it, luigi.muzzi@enea.it).

Color versions of one or more of the figures in this paper are available online at <http://ieeexplore.ieee.org>.

Digital Object Identifier will be inserted here upon acceptance.

As no thermal-hydraulic (TH) characterization was previously available for such a cable prototype, especially in view of its two-hole structure, a full-scale short sample of the wind-and-react1 (WR1) prototype conductor (the same already tested to assess its DC and AC performance [3]), has been tested in 2016 in the right leg of SULTAN at SPC, Villigen (Switzerland). It was equipped with thermometers, pressure taps, mass flow meters, a differential pressure sensor and two heaters, see Fig. 2a. The main objectives of the tests were:

- the detailed hydraulic characterization of the conductor to allow the assessment / development of the friction factor correlations to be adopted in the numerical analyses of the magnet design [5], [6],
- the TH characterization of the sample, with special reference to the identification of possible uneven temperature distributions on the cross section due to the asymmetric cooling provided by the two holes.

In the paper, the experimental results of the hydraulic and thermal-hydraulic (heat slug) tests are presented first.

Due to the lack of experimental data on the small spiral-



Fig. 1. Pictures of the CICC sample tested in SULTAN in 2016: (a) cross section and (b) whole sample length. In (b) the red markers following the two holes twisted path are also visible (see the text).

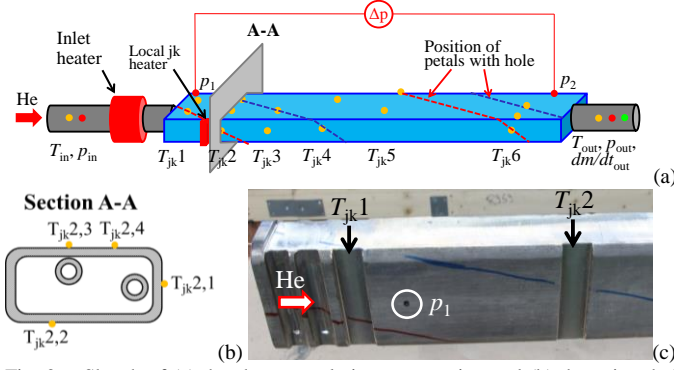


Fig. 2. Sketch of (a) the short sample instrumentation and (b) the azimuthal location of the 4 jacket temperature sensors on section A-A. (c) Picture of the conductor sample after jacket machining (vertical grooves) to fit the temperature sensors; the two markers (red and blue lines) following the projection on the conductor surface of the twisted paths of the two holes are also evident, as well as the hole where the  $p_1$  tap is installed.

walled pipe used for the two holes, a computational-fluid-dynamics (CFD) analysis is performed to derive a suitable friction factor correlation for that type of spiral. The correlation can be adopted in 1D TH codes (like e.g. the 4C code [7]) for the simulation of this kind of CICC together with existing, validated friction factor correlations for the strands bundle region [8]. The pressure drop obtained applying this set of correlations is then compared with the experimental hydraulic characterization to assess the suitability of the former in order to use it in the simulations for the pre-conceptual design analysis [9], [10].

The heat slug tests performed in SULTAN are also used to calibrate (and validate) the free parameters typically present in the models of the bundle-to-hole heat transfer, by comparing the computed temperature evolution at the different axial locations with the experimental data. An accurate assessment of these parameters is needed to accurately capture the propagation of thermal disturbances along the conductor such as, e.g., the propagation of a quench.

## II. EXPERIMENTAL SETUP

### A. Instrumentation

The sample tested in SULTAN, the main characteristics of which are listed in Table I, was well instrumented from the thermal-hydraulic point of view. The diagnostics included:

- Inlet and outlet temperature (T) and pressure (p) sensors, and outlet mass flow (dm/dt) meters (see also Fig. 3a for their exact location).
- Differential pressure sensor across 2 m of conductor length (Fig. 2a).
- Local jacket temperature (T<sub>jk</sub>) sensors.

The T<sub>jk</sub> sensors are quite peculiar of this experiment - before installing them, the poloidal position of the two petals with the hole has been carefully marked on the whole sample length, following their twisted paths, as reported in Fig. 1b and Fig. 2c. At the 6 selected axial locations reported in Fig. 3b, the jacket has been locally machined in order to reduce its thick-

TABLE I  
ENEA TF CONDUCTOR PARAMETERS [3]

Parameter	Value
Sample length	2.546 m
Jacket outer dimensions	72 mm × 38.8 mm
Jacket inner dimensions	66.6 mm × 25 mm
SC strands (number/diameter)	1080 / 1 mm
Cu strands (number/diameter)	132 / 1 mm
Cu / non Cu ratio in SC strands	1
Last cable stage twist pitch	690 mm
Cos( $\theta$ )	0.95
Bundle void fraction	24.6%
Bundle hydraulic diameter	0.336 mm
Spiral diameter (inner/outer)	4.6 mm / 6.6 mm
Spiral pitch	6.4 mm
Spiral perforated area (gap)	36% (3.83 mm)

ness to only 2.7 mm, as shown in Fig. 2c. At each location, 4 temperature sensors have been installed at different azimuthal positions on the jacket surface, namely in correspondence of the petals with the two holes and at two intermediate positions, see the sketches in Fig. 2a-b, aimed at assessing the temperature gradients that could arise on the conductor cross section following the local perturbation induced by the jacket heater.

### B. Heaters

In order to induce thermal perturbations, two heaters were installed on the sample:

- A resistive heater on the inlet pipe, shown in Fig. 4a, used to characterize the CICC hydraulic performance at different operating inlet temperatures  $T_{in}$ .
- A jacket heater, shown in Fig. 4b, right upstream of T<sub>jk2</sub> sensor, aimed at heating only a single petal, namely one of the two petals containing a hole.

## III. TEST RESULTS

The thermal-hydraulic tests performed include:

- Measurement of the steady state pressure drop for different mass flow rates at different  $T_{in}$ , aiming at the hydraulic characterization of the conductor
- Propagation of heat slug tests induced by the heater on

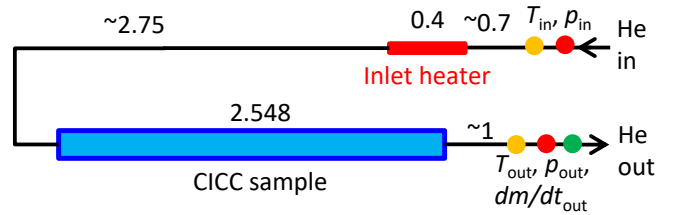


Fig. 3. Sketch of the location of (a) inlet heater,  $p$ ,  $T$  and  $dm/dt$  facility sensors, and (b) sensors installed on the sample (all quotes are in m). The inlet and outlet pipes diameter is 6 mm (inner) × 8 mm (outer).

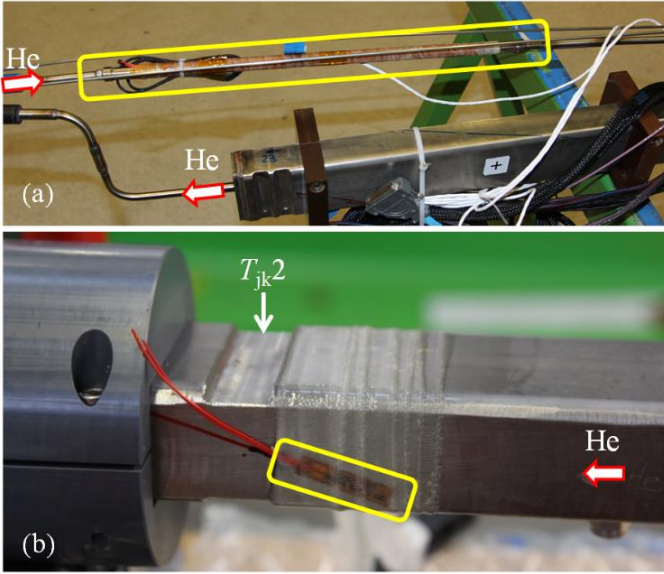


Fig. 4. Picture of the local jacket heater installed few centimeters upstream the  $T_{jk2}$  set of thermometers.

the inlet pipe, at different mass flow rates and input power, aiming at the measurement of the average He speed in the conduit

- Propagation of heat slug tests induced by the local heater on the conductor jacket, at different mass flow rates and input power, aiming at the assessment of the temperature homogenization on the conductor cross section.

A summary of the hydraulic and TH tests is reported in Table II and Table III, respectively.

#### A. Hydraulic tests

During the hydraulic tests, the mass flow rate was reduced stepwise from the maximum to the minimum values acting on a control valve. The pressure was then also changed, keeping  $T_{in}$  constant by a manual control of the inlet heater input power. These conditions were kept constant for a sufficiently long time, in order to measure the hydraulic performance only when steady state flow conditions were reached in the whole sample. The evolution of the mass flow rate and pressure drop along the conductor for a typical shot (constant  $T_{in}$ ) are reported in Fig. 5.

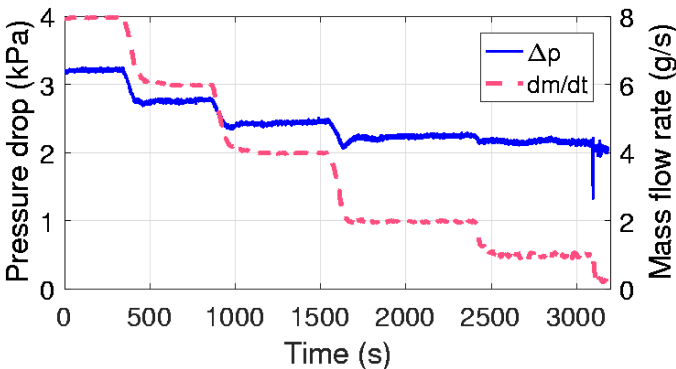


Fig. 5. Evolution of measured pressure drop (solid, left axis) and mass flow rate (dashed, right axis) for shot ENEAa180702 ( $T_{in} \sim 6$  K).

TABLE II  
SUMMARY OF HYDRAULIC TESTS

Shot	$T_{in}$ (K)	$dm/dt$ (g/s)
ENEAA180701	4.5	~0, 2, 4, 6, 8, 10
ENEAA180702	6	~0, 1, 2, 4, 6, 8
ENEAA180703	8.5	~0, 1, 2, 3
ENEAA180704	11	~0, 1, 1.5, 2
ENEAA180705	13.5	~0, 1, 1.5

TABLE III  
SUMMARY OF THERMAL-HYDRAULIC TESTS ( $T_{in} = 4.5$  K)

Shot	$dm/dt$ (g/s)	Inlet heater (W)	Jk heater (W)
ENEAb190702		20	0
ENEAb190703	7	40	0
ENEAb190704		0	10
ENEAb190705		0	15
ENEAb190706		20	0
ENEAb190707	5	40	0
ENEAb190708		0	10
ENEAb190709		0	15
ENEAb190710		20	0
ENEAb190711	3	40	0
ENEAb190712		0	10
ENEAb190713		0	15

Fig. 6 shows the measured hydraulic characteristic of the CICC sample at different temperature values. The experimental points correspond to the average value of pressure drop and mass flow rate during at least  $\sim 100$  s steady state operating conditions (the plateau in Fig. 5). The offset in the pressure drop measurement (value at  $\sim 0$  g/s) has been removed. The error bar is due to nominal  $\Delta p$  and  $dm/dt$  sensors accuracy summed to the uncertainty due to the measured signal oscillations. The progressive increase of the pressure drop at constant mass flow rate for increasing He temperature is due to the fact that (at the first order approximation)  $\Delta p \propto 1/\rho$ , where  $\rho$  is the He density, for constant  $dm/dt$ , and the density reduces of a factor  $\geq 3$  from 4.5 K to 13.5 K.

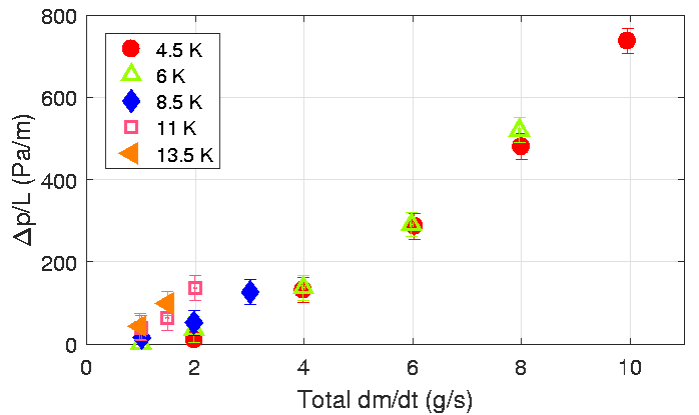


Fig. 6. Steady state experimental data collected during the sample hydraulic characterization. The error bars are due to sensors accuracy and to the uncertainty introduced by the measured signal oscillations. The mass flow rate on the x-axis is the total (bundle region + holes) mass flow rate in the CICC.



### B. Thermal-hydraulic tests

The propagation of a heat slug driven by the inlet resistive heater is shown in Fig. 7. The jacket thermometers at the same axial location (represented with the same color in Fig. 7) but at different azimuthal position are pretty consistent with each other, with some small (on average within 0.1 K, after removing the initial offset) difference. The heat slug advection from the inlet (T1.x sensors) to the sample mid-length (T6.x sensors) and to the outlet thermometer ( $T_{out}$ ) is evident from the location of the different temperature peaks. The temperature evolution at the T1.x sensors in fact resembles the square-waveform of the power deposition (40 W for 5 s, in this specific shot), while during the propagation along the sample the heat and mass transfer between holes and the bundle causes the broadening and lowering of the thermal disturbance. Note that due to a short circuit with the jacket, data from sensor T5.2 have been discarded.

The propagation of a heat slug driven by the local jacket heater is reported in Fig. 8. The  $T_{jk}$  sensors highlight that the heating is localized just upstream the  $T_{jk2}$  sensors, and precisely on the jacket surface in correspondence of the petal with the highest among all T2.x sensors, see Fig. 8a. The maximum temperature among T3.x sensors is measured by T3.3 sensor, i.e. the one measuring the  $T_{jk}$  in correspondence of the petal containing the other hole. Being the characteristic time of heat diffusion among the T2.x and T3.x sensors along the steel jacket  $\sim 1000$  s ( $\gg \sim 1$  s, the He advection time along the same distance), this implies that the (warm) He path is not that much constrained inside the twisted hole, but it can travel (and advect heat) along paths almost parallel to the conduit axis, crossing the spiral gaps and exchanging heat in an efficient way with the neighboring petals. The quasi-3D representation of the petal temperature distribution long the conduit reported in Fig. 9 confirms that the hot spot on the conductor cross section remains at the azimuthal location of the heater also in correspondence of  $T_{jk3}$  section. Moreover, from Fig. 9 it is evident that a local thermal perturbation will be redistributed across the conductor cross section, leading to a homogeneous temperature distribution, well within one twist pitch of the last cabling stage. At  $T_{jk5}$  section the temperature is indeed already uniform on the conductor cross section, at a distance  $\sim 0.45$  m (see Fig. 3b)  $< \frac{3}{4} \cdot 0.69$  m (twist pitch of the last cabling stage,

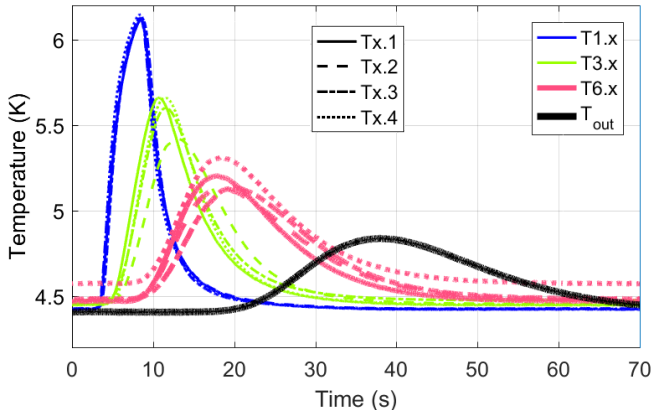


Fig. 7. Evolution of the measured temperature during heat slug test ENEAb190707.

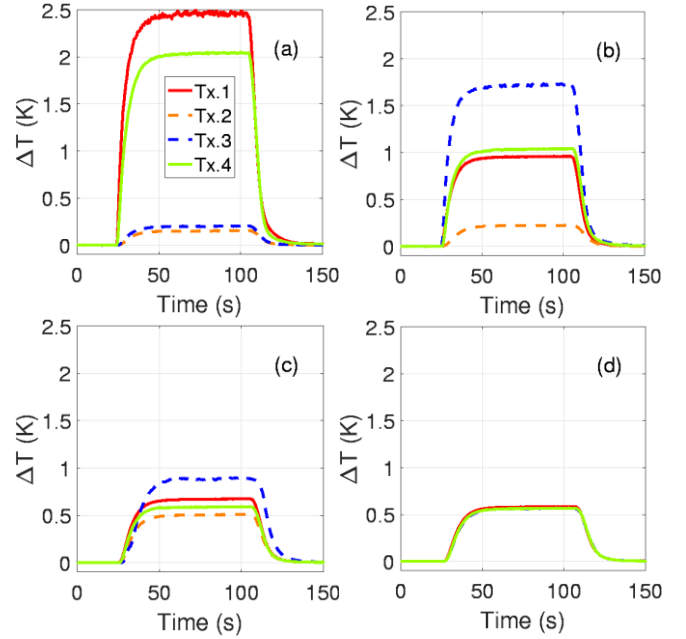


Fig. 8. Measured evolution of the jacket temperature at  $T_{jk2}$  (a),  $T_{jk3}$  (b),  $T_{jk4}$  (c) and  $T_{jk5}$  (d) during a heat slug propagation test (shot ENEAb190705), performed energizing only the local jacket heater just upstream  $T_{jk2}$ .

see Table I).

This implies that, notwithstanding the (apparently) asymmetric cooling provided by two separate holes, available 1D numerical tools are still applicable to analyze the behavior of such CICC, provided that the distance from the (local) thermal perturbation is  $> \sim$ half of the last cabling stage twist pitch.

### IV. CFD ANALYSIS OF THE HOLE

The hydraulic characterization extracted from the experiment results can be used to assess the friction factor correlations to be adopted in the TH simulations in the magnets design phase. However, while for the bundle region such correla-

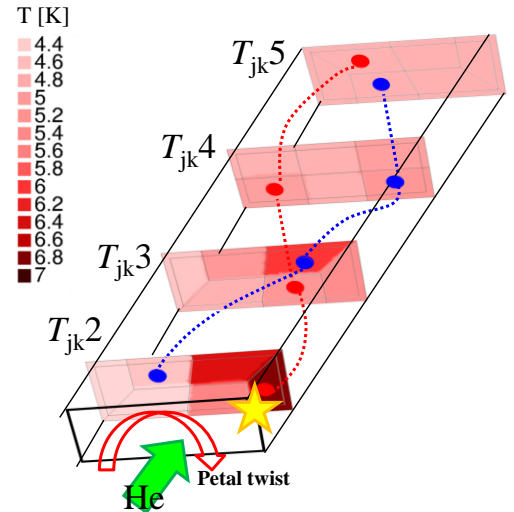


Fig. 9. Steady state temperature distribution on the different cross sections of the CICC sample during shot ENEAb190705, performed energizing only the local jacket heater (yellow star) just upstream  $T_{jk2}$ . The holes twisted paths are also reported.

tion is already available [8] and was also recently validated against experimental data not used to derive it [11], for a low-impedance channel with a flat-spiral having an inner diameter of 5 mm no correlations are available. Due to the lack of measured pressure drop data on such a small spiral, it is not possible to obtain a correlation starting from experimental data as done in the past [12]. For this reason, in this Section a Computational Fluid Dynamics (CFD) model is generated and used to perform computational experiments. The computed operating points are used to deduce the friction factor correlation for the hole, following the approach in [13], [14].

### A. CFD model

The CFD analysis of the spiral of one DEMO TF conductor has been performed using the commercial software STAR-CCM+ v11.04.012 [15].

The computational domain adopted for the analysis is a  $\sim 23$ -pitch-long portion of the hole, much longer than the single-pitch domain usually analyzed [14], to capture the periodic flow pattern induced by the spiral wall.

The spiral is assumed to be straight, even though it is twisted together with the last cabling stage. This assumption is justified by the fact that the pitch of the spiral is much smaller than the twist pitch of the last cabling stage, therefore the influence of the spiral twist in the cable on the flow field is neglected here. No mass transfer is supposed to take place between the hole and the bundle (the latter is not modeled).

The simulations have been performed using the following models:

- Pure hydraulic, 3D, steady state, incompressible flow.
- $k-\omega$  Shear Stress Transport (SST-Menter) turbulence model [16] with all  $y^+$  wall treatment
- constant properties (density  $\rho$  and dynamic viscosity  $\mu$ )

Note that the He properties were adjusted depending on the corresponding experimental He inlet temperature considered.

Concerning the mesh generation, a careful mesh independence study has been performed. The resulting mesh, shown in Fig. 10, is composed by 1.3 million of cells, including polyhedra and eight prism layers for the near-wall treatment.

### B. Simulation setup

The boundary conditions adopted for all the simulations are the following:

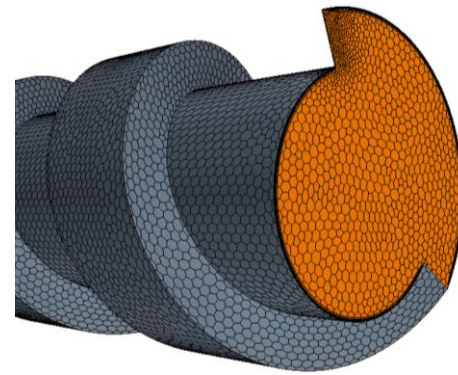


Fig. 10. Zoom of the meshed geometry (outlet region).

- Inlet: imposed mass flow rate and temperature (a uniform velocity profile is assumed at the inlet cross section)
- Outlet: zero pressure (gauge)

The inlet temperature range considered in the CFD analysis is the same of the experiment. On the other hand, we avoid to simulate all the mass flow rate values tested in the experiment if they were very close. However, we introduced, especially at high temperature (11 K and 13.5 K), additional mass flow rate values, in order to have more points and to define better the region at higher  $Re$ , which is also the DEMO operating condition, see below.

### C. Results

The velocity field resulting from the CFD analysis is presented in Fig. 11. After the entry effect that lasts for  $\sim 10$  pitches, a periodic flow field is achieved. Furthermore, the period is  $\sim 5$  pitches long and this justify the choice not to have a single pitch with periodic boundary conditions.

The periodic flow under discussion can be observed in Fig. 11b. The azimuthal location where the maximum velocity is computed on successive pitch cross sections is moving in clockwise direction (looking in the flow direction) as the fluid moves along the spiral. This secondary flow is driven by the pitch of the spiral itself, and this macroscopic motion has to be taken into account since it influences the pressure drop computation.

The Blasius friction factor ( $f_{Bl}$ ) has been obtained from the

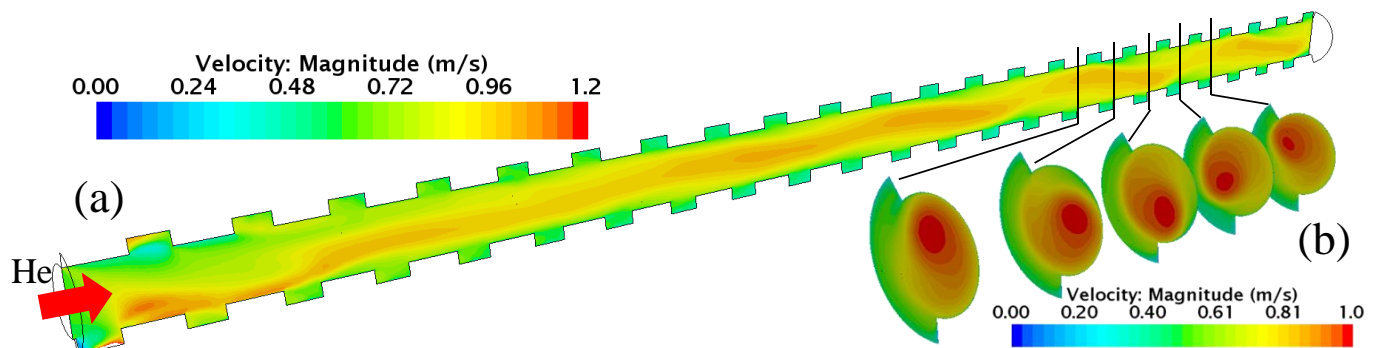


Fig. 11. (a) Velocity field on a longitudinal cross section of a hole. The inlet is located on the left. (b) Velocity field on five cross sections, distant one pitch from each other.

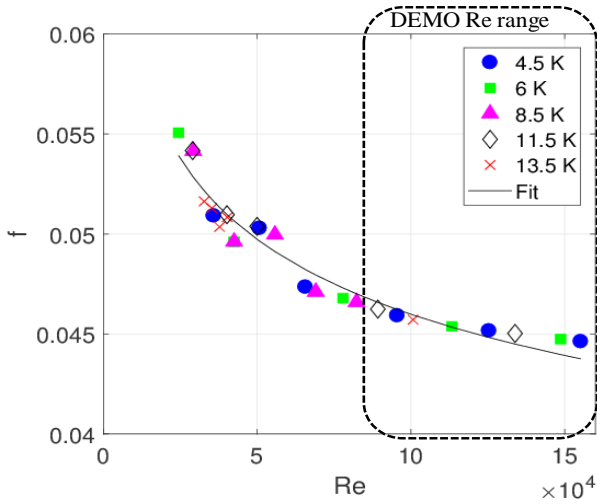


Fig. 12. Hole friction factor computed by the CFD computational experiment vs.  $Re$  for different inlet temperature values (symbols). The power-law best fit (2) is also shown, together with the foreseen DEMO operational range.

simulation using (1):

$$f_{BI} = 2 \frac{D}{L} \frac{\Delta p}{\rho v^2} \quad (1)$$

where  $D$  is the hole internal diameter, the pressure drop  $\Delta p$  has been computed across a length  $L$  equal to a 10-pitch-long period close to the outlet and the velocity ( $v$ ) has been computed as the mass flow average over the two cross sections used to evaluate the  $\Delta p$ , see Fig. 11b.

The  $f_{BI}$  values obtained from the simulations are reported as a function of the Reynolds number  $Re = \rho v D / \mu$  in Fig. 12, and they are well fitted ( $R^2 = 0.95$ ) by the power law in (2)

$$f_{BI}(Re) = 0.1687 \cdot Re^{-0.1129} \quad (2)$$

## V. THERMAL-HYDRAULIC CHARACTERIZATION

### A. Hydraulic characterization

The correlation developed by the computational (CFD) experiment in previous Section, valid for this specific spiral in the operating range tested in this experimental campaign (fully representative of the real DEMO TF coils one), is used here for the calculation of the friction factor in the two holes of the ENEA DEMO TF conductor proposal. Note that the holes have been considered circular for their entire length (as no total nor even partial collapse of the spiral during the conductor squeezing has been considered) since a CICC piece autopsy has shown a small ovality ( $\sim 1.3$ ) [3].

For the bundle region, the Darcy-Forchheimer correlation for flow in porous media [8] is adopted (with a caveat on the dependence of permeability on porosity only and not, as it should, also on the tortuosity and so on the different cabling twist pitches), according to [17]. It was developed for a wide range of bundle void fractions (between 25% and 45%) and based on an experimental database where  $10 < Re < 14000$  (for the sample during the tests, as well as in DEMO-relevant

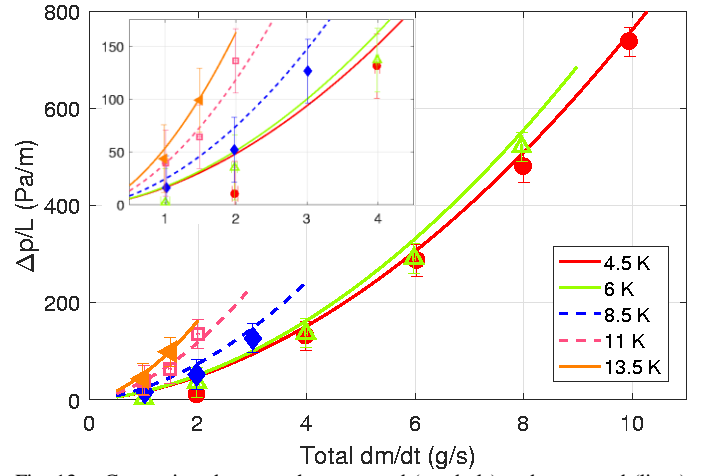


Fig. 13. Comparison between the measured (symbols) and computed (lines) hydraulic characteristic of the sample on the whole range tested in the experimental campaign; a zoom at low mass flow rates is reported in the inset. The error bars are due to sensors accuracy and to the values oscillation during data acquisition. The mass flow rate on the x-axis is the total mass flow rate in the CICC.

operating conditions,  $60 < Re < 1000$  in the bundle). The resulting characterization is compared with the experimental data collected on the CICC sample tested in SULTAN, and the result of the comparison is reported in Fig. 13 in the dimensioned ( $\Delta p$  vs.  $dm/dt$ ) plane. For all the different inlet temperatures (from the nominal value of 4.5 K up to 13.5 K) the agreement between the measurement and the characteristic predicted by the correlations is within the experimental error bar.

It is well known that the temperature wave in the conduit travels with the average He speed in the cross section. The He speed can be estimated experimentally evaluating the He transit time  $\Delta t$  between the  $T_{jk1}$  and  $T_{jk6}$  sets of sensors (estimated as the difference between the times at which the average temperature signal reaches its peak), and knowing the distance between the two ( $\Delta x$ ). The average speed  $v_{ave}$  is then estimated as  $\Delta x / \Delta t$ . Fig. 14 reports the comparison between the experimental average He speed in the conduit estimated from experimental data (see e.g. Fig. 7) and the computed one (area-weighted average of the computed bundle and hole speed). The good agreement (always within the experimental error bar) confirms that the available set of correlations is capable to capture both the hydraulic characteristic and the mass flow

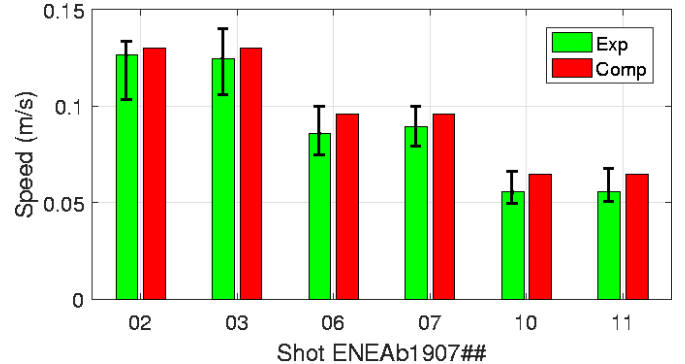


Fig. 14. Comparison between the measured (green bars) and computed (red bars) He average speed in the sample. The error bars are due to the different times at which the 4 temperature sensors at  $T_{jk1}$  and  $T_{jk6}$  reach the peak value.



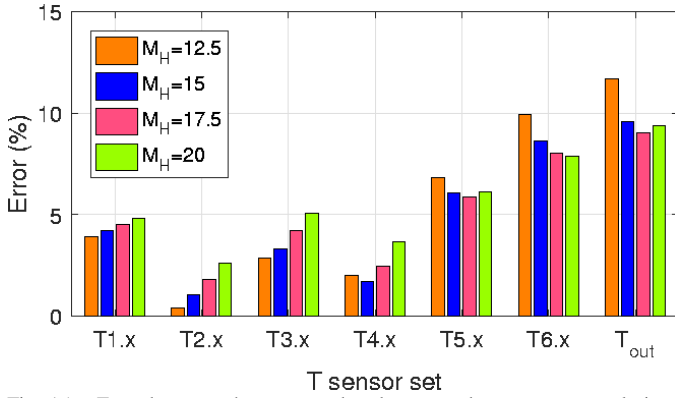


Fig. 15. Error between the computed and measured temperature evolutions at the instrumented sections of the sample during heat slug shots, used for the bundle-to-hole heat transfer multiplier ( $M_H$ ) calibration.

rate repartition between holes and bundle in the CICC (computed to be in the proportion 55%-45%, respectively), confirming the adequacy of the assumptions of circular holes everywhere.

### B. Thermal-hydraulic characterization

In view of the tight thermal coupling between the holes and the bundle, demonstrated in the experiment by the fast temperature homogenization across the conductor cross section, an accurate calibration of this heat transfer mechanism is needed by the numerical tools used for the design of the DEMO TF magnets, especially to perform reliable quench simulations [19]. Here the heat slug tests performed energizing the inlet heater are used to calibrate the above-mentioned thermal coupling in the 4C TH code [7].

In the 4C model of a DEMO TF coil, described in detail in [6], [9] and [10], the heat transfer between the two regions (holes and bundle) is computed as the parallel of two thermal resistances across the spiral, and namely: the series of hole-spiral boundary layer + spiral wall + spiral-bundle boundary layer (weighted with the unperforated fraction of spiral) and the series of hole-wall boundary layer + wall-bundle boundary layer, that qualitatively accounts for the heat transfer across

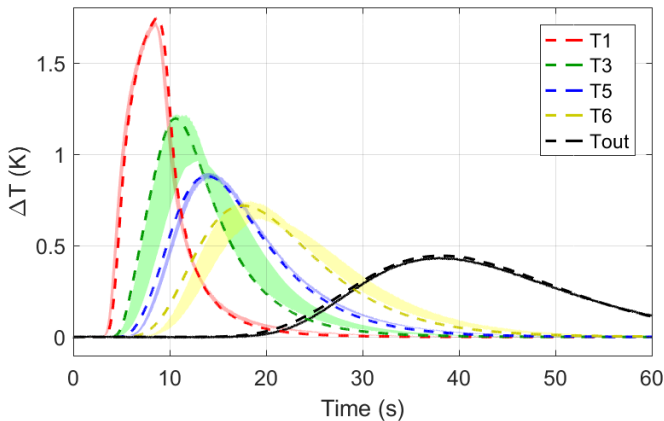


Fig. 16. Comparison between the computed and measured temperature evolutions at the instrumented sections of the sample during heat slug shot ENE-Ab190707, used for the bundle-to-hole heat transfer multiplier ( $M_H$ ) calibration. The colored areas are the envelope of the  $T_{j,k}$  sets of sensors.

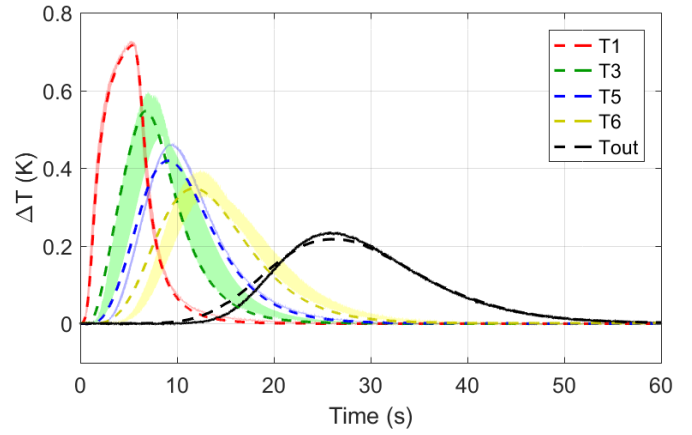


Fig. 17. Comparison between the computed and measured temperature evolutions at the instrumented sections of the sample during heat slug shot ENE-Ab190702. The colored areas are the envelope of the  $T_{j,k}$  sets of sensors.

the spiral gap (the heat transfer due to mass exchange is also separately accounted for) [20]. The heat transfer across the spiral gap is the most uncertain one, and in the model a suitable multiplier  $M_H > 1$  is included, to account for the effects of local turbulence. The calibration of  $M_H$  has been performed minimizing the average error in the computed temperature evolution at each  $T_{j,k}$  location (including also the outlet  $T$  sensor) with respect to the measured evolution. Being the latter measured at several azimuthal locations, the error has been computed as distance from the envelope of minimum and maximum temperature values measured at the same axial location.

The 4C model of the sample adopted to perform the simulations includes the sample itself and the circuit of the facility up to the  $p$ ,  $T$  and  $dm/dt$  sensors reported in Fig. 3. The simulations have been performed starting from an initial  $T$ ,  $p$  and  $dm/dt$  equal to the experimental ones. Then the experimental  $p_{in}$  and  $p_{out}$  have been prescribed as boundary conditions at the respective sensors locations, while energizing the inlet heater (also included in the model) according to the experimental power value.

The results for the scanned  $M_H$  range (from 12.5 to 20) are reported in Fig. 15. The typical value of  $M_H$  for ITER-like conductors, featuring straight low-impedance channels with a minimum inner diameter of 7 mm (Central Solenoid conductor [21]), is  $\sim 10$  (see e.g. [19]). In the present case, the  $M_H$  value for which the average value of the error on all sensors is minimized is 17.5. This larger value if compared with ITER-like conductors can be justified by a higher He turbulence in the spiral gaps, due to the increased thickness-to-diameter ratio for such a small spiral (inner diameter 5 mm, see Table I, being the 1 mm thickness unchanged). The enhanced bundle-to-hole heat transfer confirms and justifies the fast temperature homogenization on the conductor cross section following a localized thermal disturbance, see Fig. 9.

The comparison between the computed and measured temperature evolutions with the optimum  $M_H$  multiplier is reported in Fig. 16, showing an excellent agreement (average error within 5%). In order to confirm the calibration, it was validat-

ed on another heat slug shot, not used for the calibration, see Fig. 17, showing again a very good agreement.

## VI. CONCLUSIONS AND PERSPECTIVE

Dedicated thermal-hydraulic tests were performed in SULTAN in 2016 on a full-size, short length sample conductor, proposed by ENEA for the EU DEMO Toroidal Field coils. The detailed instrumentation allowed to retrieve its hydraulic characteristic and to assess that the response to an (azimuthally and axially) localized heating becomes roughly uniform on the conductor cross section at a distance of  $\sim 3/4$  of the final cabling stage twist pitch from the heater.

A set of Computational Fluid Dynamics (CFD) experiments has then been carried out in order to compute a friction factor for the hole (5 mm inner diameter). This friction factor correlation, together with the Darcy-Forchheimer correlation for the friction in the bundle region, was shown to accurately reproduce the measured hydraulic characteristic of the conductor.

The hole-to-bundle thermal coupling has also been calibrated in the 4C thermal-hydraulic code, exploiting the heat slugs performed in the sample.

In perspective, the newly developed friction factor correlation for the hole and the calibrated hole-to-bundle heat transfer multiplier will be adopted in the analysis of the ENEA proposal for the EU DEMO TF winding pack, including cyclic plasma burn and quench analyses.

## REFERENCES

- [1] L. Zani, C. M. Bayer, M. E. Biancolini, R. Bonifetto, P. Bruzzone, C. Brutti, D. Ciazynski, M. Coleman, I. Duran, M. Eisterer, W.H. Fietz, P.V. Gade, E. Gaio, F. Giorgetti, W. Goldacker, F. Gömöry, X. Grados, R. Heller, P. Hertout, C. Hoa, A. Kario, B. Lacroix, M. Lewandowska, A. Maistrello, L. Muzzi, A. Nijhuis, F. Nunio, A. Panin, T. Petrisor, J-M. Poncet, R. Prokopec, M. Sanmarti Cardona, L. Savoldi, S.I. Schlachter, K. Sedlak, B. Stepanov, I. Tiseanu, A. Torre, S. Turtù, R. Vallcorba, M. Vojenciak, K.-P. Weiss, R. Wesche, K. Yagotintsev, and R. Zanino, "Overview of Progress on the EU DEMO Reactor Magnet System Design", *IEEE Trans. Appl. Supercond.*, vol. 26, no. 4, Jun. 2016, Art. no. 4204505.
- [2] V. Corato, M. E. Biancolini, R. Bonifetto, P. Bruzzone, D. Ciazynski, M. Coleman, A. della Corte, A. Dembkowska, M. Eisterer, W.H. Fietz, E. Gaio, F. Giorgetti, R. Heller, B. Lacroix, M. Lewandowska, A. Maistrello, L. Muzzi, A. Nijhuis, F. Nunio, A. Panin, L. Savoldi, K. Sedlak, B. Stepanov, G. Tomassetti, A. Torre, S. Turtù, D. Uglietti, A. Vaccaro, R. Vallcorba, K.-P. Weiss, R. Wesche, M. Wolf, L. Zani, and R. Zanino, "EU Progress in Superconductor Technology Development for DEMO Magnets," to be presented at ISFNT (2017).
- [3] L. Muzzi, L. Affinito, S. Chiarelli, V. Corato, A. della Corte, A. Di Zenobio, R. Freda, S. Turtù, A. Anemona, R. Righetti, A. Bragagni, M. Seri, F. Gabiccini, G. Roveta, A. Aveta, S. Galignano, P. Bruzzone, K. Sedlak, B. Stepanov, and R. Wesche, "Design, Manufacture, and Test of an 80 kA-Class Nb<sub>3</sub>Sn Cable-In-Conduit Conductor With Rectangular Geometry and Distributed Pressure Relief Channels," *IEEE Trans. Appl. Supercond.*, vol. 27, no. 4, Jun. 2017, Art. no. 4800206.
- [4] K. Kim, S. Oh, J. S. Park, C. Lee, K. Im, H. C. Kim, G.-S. Lee, G. Neilson, T. Brown, C. Kessel, P. Titus, and Y. Zhai, "Conceptual design study of the K-DEMO magnet system", *Fus. Eng. Des.*, vol. 96-97, 2015, pp. 281-285.
- [5] M. Lewandowska, K. Sedlak, and L. Zani, "Thermal-Hydraulic Analysis of the Low- $T_c$  Superconductor (LTS) Winding Pack Design Concepts for the DEMO Toroidal Field (TF) Coil," *IEEE Trans. Appl. Supercond.*, vol. 26, no. 4, Jun. 2016, Art. no. 4205305.
- [6] R. Zanino, R. Bonifetto, O. Dicuonzo, L. Muzzi, G. F. Nallo, L. Savoldi, and S. Turtù, "Development of a Thermal-Hydraulic Model for the European DEMO TF Coil," *IEEE Trans. Appl. Supercond.*, vol. 26, no. 3, Apr. 2016, Art. no. 4201606.
- [7] L. Savoldi Richard, F. Casella, B. Fiori, and R. Zanino, "The 4C code for the cryogenic circuit conductor and coil modeling in ITER," *Cryogenics*, vol. 50, no. 3, Mar. 2010, pp. 167-176.
- [8] M. Bagnasco, L. Bottura, and M. Lewandowska, "Friction factor correlation for CICC's based on a porous media analogy," *Cryogenics*, vol. 50, 2010, pp. 711-719.
- [9] L. Savoldi, R. Bonifetto, A. Brighenti, V. Corato, L. Muzzi, S. Turtù, and R. Zanino, "Performance analysis of a graded winding pack design for the EU DEMO TF coil in normal and off-normal conditions," to appear in *Fus. Eng. Des.*, 2017.
- [10] L. Savoldi, R. Bonifetto, A. Brighenti, V. Corato, L. Muzzi, S. Turtù, R. Zanino, and A. Zappatore, "Quench propagation in a TF coil of the EU DEMO," *Fus. Sci. Technol.*, 2017.
- [11] A. Brighenti, R. Bonifetto, T. Isono, K. Kawano, G. Russo, L. Savoldi, and R. Zanino, "Overview of the hydraulic characteristics of the ITER Central Solenoid Model Coil conductors after 15 years of test campaigns," to appear in *Adv. Cryo. Eng.*, 2017.
- [12] R. Zanino, P. Santagati, L. Savoldi Richard, A. Martinez, and S. Nicollet, "Friction factor correlation with application to the central cooling channel of cable-in-conduit super-conductors for fusion magnets," *IEEE Trans. Appl. Supercond.*, vol. 10, 2000, pp. 1066-1069.
- [13] R. Zanino, S. Giors and L. Savoldi Richard, "CFD modeling of ITER cable-in-conduit superconductors. Part III: correlation for the central channel friction factor," *proceedings of the 21th International Cryogenic Engineering Conference (ICEC21)*, vol. 1, 2007, pp. 207-211.
- [14] R. Zanino, S. Giors, and R. Mondino, "CFD Modeling of ITER Cable-in-Conduit Superconductors. Part I: Friction in the Central Channel," *Adv. Cryo. Eng.*, vol. 823, no. 1, May 2006, pp. 1009-1016.
- [15] Star-CCM+ User's Manual 11.04, CD ADAPCO, New York, 2016.
- [16] F. R. Menter, "Review of the shear-stress transport turbulence model experience from an industrial perspective," *Int. J. Comput. Fluid Dyn.*, vol. 23, no. 4, 2009, pp. 305-316.
- [17] L. Savoldi, and R. Zanino, "Common approach for thermal-hydraulic calculations," *EFDA\_D\_2LMECE*, v1.2, 16/09/2016.
- [18] L. Muzzi, and A. Di Zenobio, "Fabrication of two short length TF conductor section, RW1 and WR1," *EFDA\_D\_2MA95F*, 20/05/2015.
- [19] R. Bonifetto, T. Isono, N. Martovetsky, L. Savoldi, and R. Zanino, "Analysis of Quench Propagation in the ITER Central Solenoid Insert (CSI) Coil," *IEEE Trans. Appl. Supercond.*, vol. 27, no. 4, Jun. 2017, Art. no. 4700308.
- [20] R. Zanino, S. De Palo, and L. Bottura, "A two-fluid code for the thermohydraulic transient analysis of CICC superconducting magnets," *J. Fus. Energy*, vol. 14, 1995, pp. 14-25-40.
- [21] T. Isono, K. Kawano, H. Ozeki, H. Kajitani, N. Koizumi, K. Okuno, T. Minato, H. Nishimiya, Y. Watabe, H. Sakamoto, T. Sasaki, A. Smirnov, and N. Martovetsky "Fabrication of an Insert to Measure Performance of ITER CS Conductor", *IEEE Trans. Appl. Supercond.*, vol. 25, no. 3, Jun. 2015, Art. no. 4201004.